Detectability of Regional Ventricular Conduction Slowing from ECGs under Baseline Activation Variability

Julia Camps, Oscar Camara

Universitat Pompeu Fabra, Barcelona, Spain

Abstract

Regional ventricular conduction slowing changes QRS morphology, but its ECG visibility may depend on the healthy activation used as reference. We studied three representative synthetic ventricular anatomies with ten selected healthy activation baselines per anatomy. Each healthy baseline was compared with 27 slowed variants spanning three regions, three spatial extents and three slowing severities, giving 810 matched comparisons. Change was assessed using mean Pearson correlation coefficient (PCC) across leads I, II and V1–V6 and the minimum lead-wise PCC, representing the most affected analysed lead; lower PCC indicates greater change. Stronger slowing always and larger slowed regions almost always produced larger morphology changes, whereas the relative effects of the tested regional perturbations were less stable across baselines and more baseline-dependent in individual leads than after averaging across leads. At the largest tested extent and strongest slowing, with conduction speed reduced to 40% of baseline, anterior-mid produced the largest lead-specific change in 27 of 30 baselines and anterior-apical in three. ECG-based digital twins should therefore assess regional slowing across plausible healthy activation solutions rather than treat one fitted-baseline response as uniquely determined.

1. Introduction

ECG-based cardiac digital twins integrate clinical observations with mechanistic models but may admit several healthy-compatible parameterisations [1, 2]; the model-predicted QRS response to local ventricular conduction slowing can therefore depend on the underlying activation sequence [3, 4].

A response averaged across baselines can conceal whether a regional perturbation is expressed similarly in each baseline or individual lead. It is therefore important to distinguish effects that remain directionally consistent across healthy activation variability from regional or lead-specific effects that depend more strongly on the chosen reference activation.

We assessed how robust the ECG effects of slowing severity, spatial extent and three tested regional perturbations were to selected healthy baseline activation variability. Each slowed ECG was compared directly with its matched healthy baseline, allowing severity and extent consistency to be evaluated alongside baseline dependence in regional and lead-specific responses.

2. Methods

2.1. Study design

We used VAE_case_5, VAE_case_10 and VAE_case_20 from a public synthetic biventricular mesh dataset [5]. For each anatomy, healthy activation populations were calibrated to healthy QRS duration, axis, R/S progression, transition and notching. Deterministic farthest-point sampling based on pairwise centred local-activation-time (LAT) map RMSE selected ten baselines per anatomy to span activation diversity. We applied 27 perturbations to each baseline (three regions $\times$ three extents $\times$ three slowing severities), giving 810 comparisons. Every slowed ECG was compared with its corresponding healthy baseline using the same anatomy and electrode configuration.

2.2. Activation and ECG models

Sinus-rhythm ventricular activation was simulated with the established graph-based Eikonal model using Dijkstra's algorithm, orthotropic myocardial conduction and root-node activation times from a rule-based Purkinje network [4]. QRS complexes were generated from step-function transmembrane potentials using a tetrahedral pseudo-ECG formulation under an infinite homogeneous volume-conductor approximation [3]. Each anatomy used one fixed donor-derived electrode configuration. The selected baselines span healthy-compatible activation diversity and are not posterior samples.

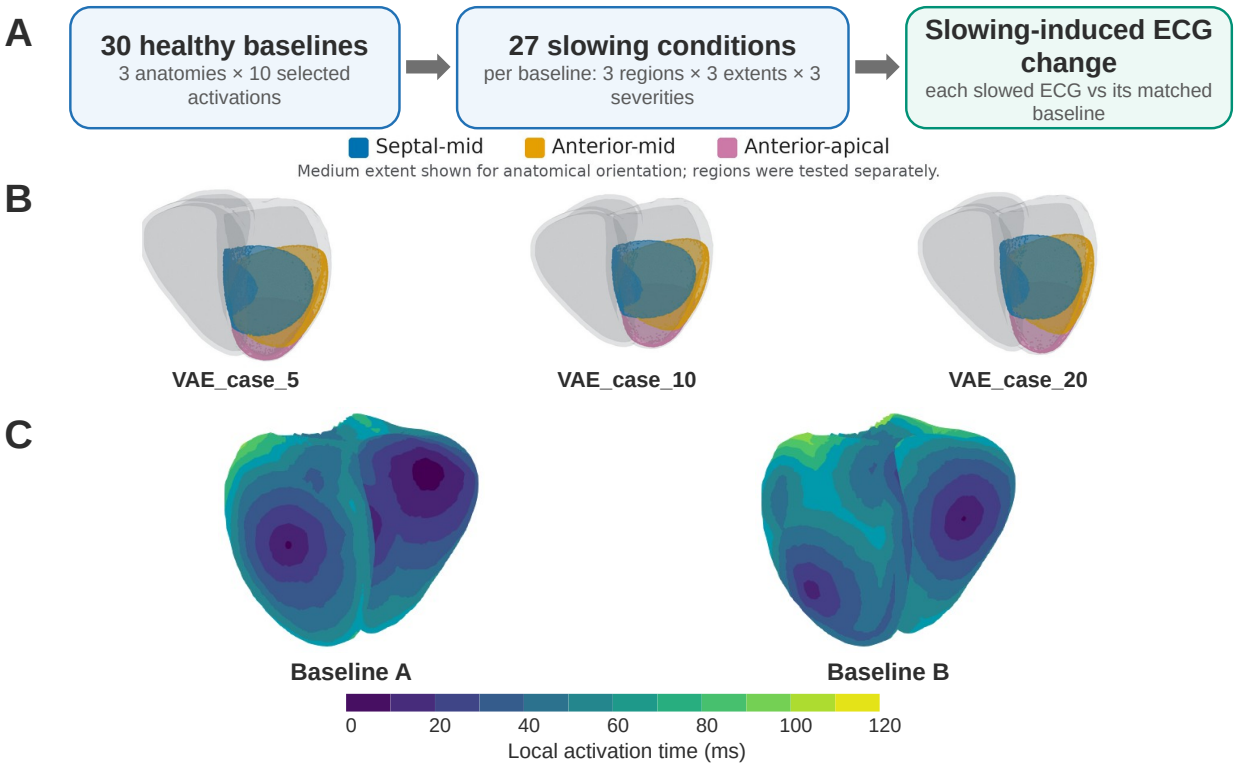

Figure 1. Study design and analysed inputs. (A) Thirty healthy baselines—ten selected activation configurations in each of three VAE anatomies—were evaluated under 27 regional-slowing conditions, with each slowed ECG compared with its matched healthy baseline. (B) VAE_case_5, VAE_case_10 and VAE_case_20 in a common view and magnification, with the three medium-extent mid-wall masks shown together for anatomical orientation; regions were tested separately and all extents were analysed. (C) The two selected VAE_case_10 activation patterns with the greatest whole-ventricle centred-LAT separation (RMSE, 22.6 ms), displayed on a shared 0–120 ms scale with 10-ms bands.

2.3. Regional slowing

We introduced slowing in three pre-specified left-ventricular mid-wall regions defined in ventricular coordinates: septal-mid, anterior-mid and anterior-apical. Small, medium and large ellipsoidal masks around each fixed centre defined the three spatial extents. Within a region, affected-edge conduction speeds were retained at 80%, 60% or 40% of baseline ($\alpha = 0.8$, 0.6 or 0.4, respectively). Septal-mid versus anterior-mid changed rotational position at the same apicobasal level, whereas anterior-mid versus anterior-apical changed apicobasal position. The nominal extents did not affect equal myocardial fractions: median fractions across anatomies ranged from 3.3–10.2% for anterior-apical, 6.0–18.5% for anterior-mid and 3.9–13.5% for septal-mid. Regional contrasts therefore describe the tested perturbations rather than pure location effects.

2.4. Metrics and analysis

We measured overall morphology change using mean PCC across the eight independent analysed leads (I, II and V1–V6), where lower PCC denotes greater change. The most-affected-lead representation was

$$M_{\text{lead}} = 1 - \min_{\ell} \text{PCC}_{\ell},$$

where $\ell \in \{\text{I}, \text{II}, \text{V1}, \ldots, \text{V6}\}$; larger M_{lead} indicates greater change in the most affected analysed lead. Matched QRS traces were compared sample-by-sample after the established filtering and normalisation pipeline, without temporal realignment or resampling. For each region–extent–severity condition, we first calculated the median metric value across the ten baselines separately within each anatomy, producing three anatomy-level medians. We then reported the median of those three medians as the cross-anatomy summary, so each anatomy contributed equally rather than pooling all 30 baselines directly. Severity comparisons held anatomy, baseline, region and extent fixed; extent comparisons held anatomy, baseline, region and severity fixed. All ordering comparisons used unrounded full-precision values. The difference in latest ventricular activation time (ΔmaxLAT) was retained as a secondary metric.

2.5. Reproducibility

Upon publication, we will release a citable Zenodo archive containing the code, frozen derived results and verification materials needed to reproduce the reported analyses and figures.

3. Results

3.1. Severity and extent

Stronger slowing produced larger ECG morphology changes in every severity comparison for both mean PCC and M_{lead}. Increasing the slowed spatial extent did so in every mean-PCC comparison and almost every M_{lead} comparison; Figure 2A shows the M_{lead} pattern.

3.2. Regional and lead-specific baseline dependence

The relative effects of the tested regional perturbations varied more across baselines than the effects of severity and extent. Under the primary sample-by-sample PCC analysis, at the largest extent and strongest slowing, anterior-mid produced the largest M_{lead} in 27 of 30 baselines and anterior-apical in three (Figure 2B). In the two highlighted cases, anterior-apical exceeded anterior-mid in V4–V5, whereas most leads and the across-lead mean retained a larger anterior-mid effect.

The two coloured trajectories in Figure 2B show the two largest exceptions to the predominant regional pattern: in these two baselines, anterior-apical slowing produced a larger M_{lead} change than anterior-mid slowing. To test whether these highlighted differences could be explained by a common whole-ECG temporal shift rather than lead-specific morphology change, we compared each full eight-lead ECG pair after one common global lag and across 24 predefined common multilead windows varying signal construction, threshold and persistence. Across the tested onset definitions, detected global onset differences were small (approximately 1–3 ms). For the larger highlighted case, anterior-apical remained above anterior-mid after the common lag and in all 24 alternative windows; for the smaller highlighted case, this relation persisted after the common lag and in 21 of 24 windows. These results argue against gross temporal misalignment while showing some waveform-window sensitivity for the smaller case.

Across the full campaign, global activation timing was almost unchanged: only 11 of 810 comparisons had non-

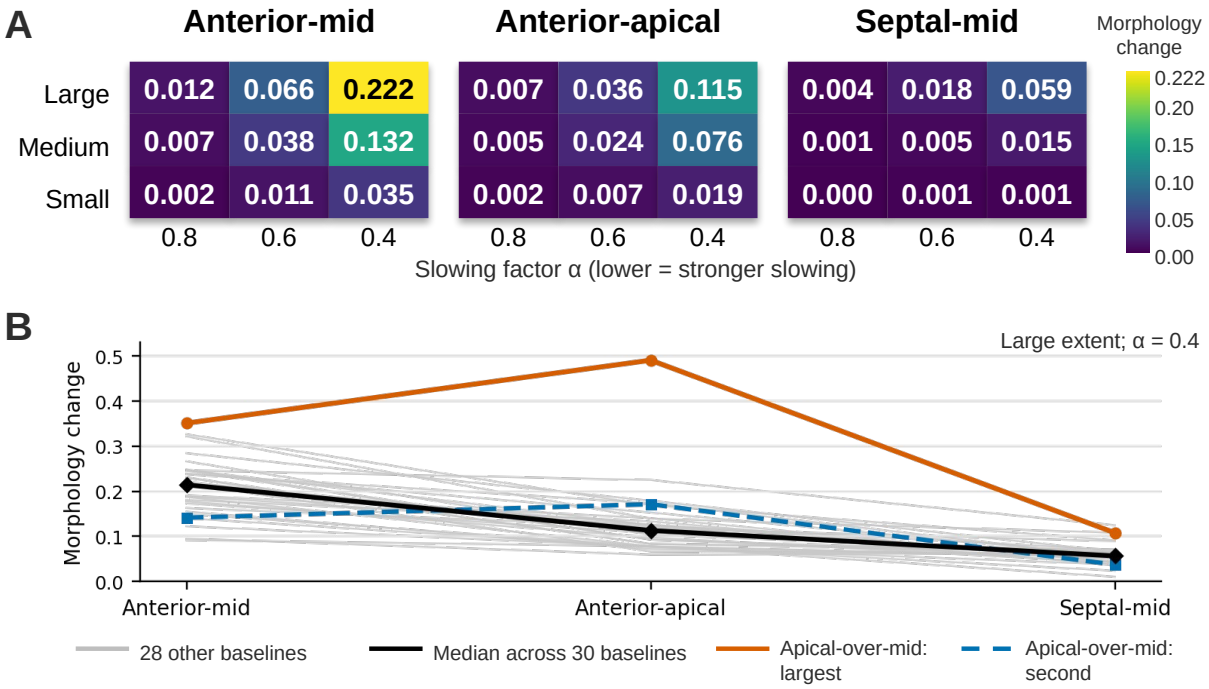

Figure 2. Most-affected-lead morphology change, $M_{\mathrm{lead}} = 1 - \min_{\ell}(\mathrm{PCC}_{\ell})$, over leads I, II and V1–V6; the most affected lead was selected separately for each comparison. (A) Medians across ten baselines within each anatomy, followed by the median across the three anatomy-level medians. (B) Individual baseline-resolved responses at the largest extent and strongest slowing ($\alpha = 0.4$; conduction speed 40% of baseline); the black line is the direct median across all 30 values and is distinct from the Panel A statistic. Counts reflect the primary sample-by-sample PCC analysis: anterior-mid produced the largest change in 27 baselines and anterior-apical in three. Coloured trajectories highlight the two largest anterior-apical-over-anterior-mid differences.

zero ΔmaxLAT, ranging from +1 to +8 ms.

4. Discussion

The direction of the severity effect was consistent across all selected healthy activation baselines, and the extent effect was almost as consistent, whereas the relative regional and individual-lead responses were more baseline-dependent. The monotonic severity and extent trends are expected; their value here is as a stable internal reference that makes the lesser stability of regional and lead-specific expression visible.

Selecting the most affected lead exposed stronger local morphology differences but also greater dependence on baseline activation, whereas averaging across leads was more stable but could dilute local effects. The highlighted cases support baseline-dependent regional and lead-specific expression without identifying a unique mechanism. In an ECG-based digital twin, different healthy-compatible activation solutions can therefore predict different response magnitudes or lead distributions for the same candidate slowing substrate. If these model-predicted responses are compared with a follow-up ECG acquired after a suspected conduction change, the selected baseline solution could alter the estimated slowing severity or the relative support for regional hypotheses. We did not perform this inverse inference, but the forward response on which it would depend was baseline-conditional. The near-unchanged latest activation time shows that local morphology can change with little alteration in global timing.

The three sentinel regions do not provide a ventricular location map, but they are sufficient to demonstrate baseline-dependent regional contrasts. Unequal affected fractions prevent a pure location-only interpretation of exact regional rankings, while within-region severity and extent comparisons remain supported. The selected baselines represent controlled healthy-compatible diversity rather than a population or posterior distribution, so no prevalence claim follows; fixed electrodes and absent measurement noise also leave exact lead patterns and clinical detectability unresolved without weakening the controlled baseline-dependence result. The study does not establish localisation, inverse recoverability or a clinical threshold; a useful next question is where regional and lead-specific effects remain stable across activation solutions and whether that stability persists under electrode-placement and noise uncertainty.

5. Conclusion

Across selected healthy-compatible activation baselines, the ECG effects of slowing severity and extent were more consistent than the relative effects of the tested regional perturbations and their expression in individual leads. ECG-based digital twins should therefore evaluate regional slowing across plausible activation solutions rather than treat the response from a single fitted baseline as uniquely determined.

Acknowledgements

The project that gave rise to these results received the support of a fellowship from 'la Caixa' Foundation (ID 100010434) to JC (LCF/BQ/PI25/12100029).

OpenAI ChatGPT was used to assist with code adaptation, result collation, figure preparation and manuscript drafting; all outputs were reviewed and verified.

References

[1] Corral-Acero J, Margara F, Marciniak M, Rodero C, Loncaric F, Feng Y, et al. The Digital Twin to enable the vision of precision cardiology. European Heart Journal 2020; 41(48):4556–4564. Doi:10.1093/eurheartj/ehaa159.

[2] Gillette K, Gsell MAF, Prassl AJ, Karabelas E, Reiter U, Reiter G, Grandits T, Payer C, Stern D, Urschler M, Bayer JD, Augustin CM, Neic A, Pock T, Vigmond EJ, Plank G. A framework for the generation of digital twins of cardiac electrophysiology from clinical 12-leads ECGs. Medical Image Analysis 2021;71:102080. Doi:10.1016/j.media.2021.102080.

[3] Camps J, Lawson B, Drovandi C, Minchole A, Wang ZJ, Grau V, Burrage K, Rodriguez B. Inference of ventricular activation properties from non-invasive electrocardiography. Medical Image Analysis 2021;73:102143. Doi:10.1016/j.media.2021.102143.

[4] Camps J, Berg LA, Wang ZJ, Sebastian R, Riebel LL, Doste R, Zhou X, Sachetto R, Coleman J, Lawson B, Grau V, Burrage K, Bueno-Orovio A, Weber dos Santos R, Rodriguez B. Digital twinning of the human ventricular activation sequence to clinical 12-lead ECGs and magnetic resonance imaging using realistic Purkinje networks for in silico clinical trials. Medical Image Analysis 2024;94:103108. Doi:10.1016/j.media.2024.103108.

[5] Doste R, Camps J, Wang ZJ, Berg LA, Holmes M, Smith H, Rodriguez B. Synthetic biventricular heart meshes generated by the InSilicoHeartGen pipeline for electromechanical simulations. Zenodo dataset, 2025. Doi:10.5281/zenodo.15372896.

Address for correspondence:

Julia Camps.
Tanger building, Tanger, 122-140, Barcelona, Spain.
julcamps@gmail.com